How can we determine the regional strike angle from a given magnetotelluric dataset ?

Hiroaki TOH[1] and Makoto UYESHIMA[2]

[1] *Ocean Research Institute, University of Tokyo. Tokyo 164 Japan*
[2] *Earthquake Research Institute, University of Tokyo, Tokyo 113 Japan*

(28/FEB/'95)

Conventional magnetotelluric (MT) analyses of the PNG dataset have revealed that it is 'very good two-dimensional (2D)' dataset with relatively high S/N ratios down to 10^{-2} Hz. It is '2D' along the direction of the profile (NNE) although traditional Swift's angles are unstable at some sites and slightly differ site by site. This implies that weak but siginificant distortions are present at all sites. Hence, the site-independent regional 2D strike angle was sought by minimizing the sum of the χ^2 misfits derived from frequency-independent Groom-Bailey (GB) decomposition at seven selected sites, which yielded a strike angle of 30° clockwise from the north. It is noteworthy that exclusive application of existing decomposition schemes to every MT dataset can become very dangerous especially when the dataset is contaminated by large χ^2 misfits at some sites. It, however, can be circumvented by rigorous and statistical examination of validity of the specific application of the existing decomposition scheme.

1. Introduction

In this paper, we present decomposition study of the PNG dataset based on three-step GB decomposition. The PNG dataset is a compact 10-site MT data collected around middle south-east of Papua New Guinea on a profile as short as 5.6 km oriented along the north-northeast direction. Its frequencies are wide enough to be more than five decades ranging from 384 Hz to 1820 sec although the ULF responses at periods longer than 100 sec are not very significant as easily understood by their large error bars. Our interest was focused upon how precisely the regional 2D strike angle can be determined by the existing decomposition scheme. In other words, our intent was to show how a specific MT dataset can be modeled totally by the existing 'physically simple but state-of-the-art' decomposition schemes to yield a reliable regional 2D strike angle esimate.

In interpretations of magnetotellurics, it is essential to derive 'good' 1D or regional 2D responses from the observed EM responses since it is sometimes still difficult to interpret them directly by three-dimensional (3D) EM modelling and/or inversion. Recently, removal of 3D surface distortions based on a rather simple physical model appeared in numerous literatures such as BAHR (1988), GROOM and BAILEY (1989), BAHR (1991), GROOM and BAILEY (1991), GROOM and BAHR (1992), GROOM *et al.* (1993) and so on. As a result, MT data collected at a specific site can be modeled very well by either frequency-dependent or frequency-independent GB decomposition even in the presence

of very strong 3D distortions as in the BC87 dataset (JONES *et al.*, 1993). However, site-independent GB decomposition for a whole dataset has never been conducted although it will be particularly of use for a compact and local dataset like the PNG dataset.

We provide a brief introduction of the PNG dataset, followed by the presentation of frequency-dependent and/or frequency-independent GB decomposition of the observed MT responses at each site. Then, the 10 reginal 2D strike angle estimates from frequency-independent GB decomposition at each site were statistically examined to show three of them were insignificant. Finally, the true regional 2D strike angle was sought by site-independent GB decomposition of the observed MT responses which minimized global χ^2 misfits derived from frequency-independent GB decomposition at seven selected site.

2. Data

The PNG dataset is a very compact MT data consisting of 10-site MT impedance tensors collected in the middle south-east part of Papua New Guinea. Length of the traverse line is as short as approximately 5.6 km lying in the SSW-NNE direction (Fig. 1). Observation was conducted at up to 40 frequencies ranging from 384 Hz to 1820 sec though large error bars at low frequencies indicated that impedances in the ULF band were not very reliable. Hence, only EM responses down to 909.9 sec, i.e., 38 frequencies were considered in this study. Tipper values were not incorporated in our analysis either since the distributed tippers showed large scatter and less consistency with MT impedances, which is presumably due to failure in Bz measurements. Traditional skewness are well below or around 0.2 except for low extreme frequencies and site PNG121, which, in addition to very small Zxx's and Zyy's, suggest that the PNG dataset is '2D' in its nature and very suitable, if precise regional 2D EM responses are derived, for constructing a detailed regional 2D electrical conductivity structure beneath the region concerned since the degree of freedom of all the regional 2D EM responses will amount to around 1400 even if the bad frequencies and site are eliminated.

The regional 2D strike angle of the PNG dataset was found to roughly coincide with the direction of the profile (SSW-NNE). For example, the traditional Swift's angles at site PNG101 in Fig. 2 (lowerleft) have been frequency-independently determined around 60° anticlockwise from the north though they still include the 90° ambiguity. However, as is offten the case with magnetotellurics, the regional strike angle is the most unstable parameter differing site by site and being frequency-dependent (JONES and GROOM, 1993). Figure 3 shows Swift's angles at site PNG104 as well as traditional skewness, polar diagrams and anisotropy ellipses, that are quite unstable in this frequency range. We, therefore, judged that the MT impedance tensors of the PNG dataset were subject to weak but significant near-surface 3D distortion and decided to apply GB decomposition to the PNG dataset.

One more thing that should be mentioned here in terms of outstanding features of the PNG dataset is 'phase anomaly' between 10^{-1} to 10 Hz where TM phases become very 'high' and sometimes hit the causal bound (90°). Figure 4 shows the typical manifestation of the phase anomaly. It is very difficult to interpret this anomaly by 1D and/or 2D modelling other than introducing 'anisotropy' as had been presented by Eisel at MT-DIW2 in Cambridge provided that this anomaly is caused by a 'real' structure. This problem will be further discussed later in this paper.

3. Decomposition

GB decomposition of the PNG dataset was carried out by the following three steps using Groom and Bailey's decomposition code that was made available to us via mt-net.europe. First, frequency-dependent GB decomposition at each site was conducted. Then, we proceeded to frequency-independent GB decomposition at each site through which ten 2D regional strike angle estimates were obtained. Finally, one site- and frequency-independent 2D regional strike angle was sought by site-independent GB decomposition of the whole dataset, which minimized global χ^2 misfits. Only electric field distortion was considered in any of our GB decompositions presented here.

3.1 Frequency-Dependent GB Decomposition

Frequency-dependent GB decomposition, which allows the decomposition parameters such as twist, shear and regional strike angles to vary in the frequency domain, usually gives smaller χ^2 misfit at each site (Fig. 5a) than frequency-independent GB decomposition while, as a matter of course, the 2D regional strike angle at the specific site is not 'regional' but still 'local' being severely dependent on frequency. The frequency-dependent 2D strike angles are often very unstable even if the twist and shear angles, though these two angles tend to mirror each other, are relatively stable in the frequency range (Fig. 5b). Visual fit to the observed data (Fig. 5c) clearly shows that predicted values from frequency-dependent GB decomposition are likely to follow every data point including outliers. It is noteworthy that it may be useful to build in robustness in our decomposition schemes though elimination of simple isolated outliers can now be easily accomplished in the course of response function estimation using robust codes.

3.2 Frequency-Independent GB Decomposition

Then, the decomposition parameters were fixed in the frequency range concerned. Naturally, this gave larger χ^2 misfits and the 2D regional strike angle estimates were still 'local' in the sense that they differed site by site even though they're no longer frequency-dependent. Figure 6 shows the site-dependency of the 2D regional strike angle estimates of all the site. It is evident from the figure that those at sites PNG102, PNG121 and PNG122 are outliers falling below 0°. Site PNG121 can be excluded from determination of the true 2D regional strike angle since the traditional skewness at this site are very large as was pointed out in the previous section while it is not trivial why the 2D regional strike angle estimates at sites PNG102 and PNG122 show very different behavior from those of the remaining seven sites. To clarify this, the χ^2 misfits of all the ten sites were statistically examined. Figure 7 shows the result of the examination. We used complex full MT tensor of 38 frequencies, which means the degree of freedom of the χ^2 distribution is 304 and hence the variance is equal to 608. The horizontal line in Fig. 7 denotes the 3σ allowance. It is clear from Fig. 7 that the χ^2 misfits at sites PNG102, 121 and 122 are too large to be considered as obeying the χ^2 distribution. This implies that the 3D surface distorsion at the three sites were not successfully modeled by the 'physically-too-simple' GB decomposition scheme. Hence, these three sites were regarded as statistically insignificant and omitted from the subsequent determination of the true 2D regional strike angle.

3.3 Site-Independent GB Decomposition

Finally, a site-independent 2D regional strike angle was sought by temporarily fixing the strike angle in application of frequency-independent GB decomposition to the seven selected sites, calculating sum of χ^2 misfits of the seven sites using all frequencies and changing the temporarily fixed strike angles from 0° through 90° by 1° interval. Figure 8 shows the result of the search. The global minimum of the sum of the χ^2 misfits was found at the angle of 30° clockwise from the north. This strike angle coincided well with the direction of the profile which had been placed perpendicular to the already known geological strike. This angle was then regarded as the 2D regional strike angle of the PNG dataset and used in our successive 1D and/or 2D analyses though they were not included in this particular paper. Visual fit to the observed data using this regional strike angle was not much worsen even for the omitted site PNG102 as shown in Fig. 9.

4. Discussion

Difficulty associated with determination of the true regional 2D stike angle in MT studies may be circumvented by applying any decomposition schemes available at present to a given dataset and minimizing the global χ^2 misfit described in the previous section. However, the simple misfit minimization as presented in this paper in search for the true regional 2D strike angle estimate can be extended to more complex regulated minimizations like ABIC minimization (cf. UCHIDA, 1993) utilizing a priori information that the true regional 2D strike angle, if any, should be site- and frequency-independent, or, in a more practical sense, differ very slightly site by site and in the frequency domain. Such regulated minimization is likely to give more stable estimates of the true 2D strike angle than the simple misfit minimization even for a more distorted dataset, which is not the case with the PNG dataset.

As for the TM phase anomaly found in the frequency range from 10^{-1} to 10 Hz, it would be better not to considered it as of natural origin since it could not be reproduced in any of our 1D inversions and/or 2D forward modellings (Not shown in this particular paper. Refer to TOH and UYESHIMA (1995) for details.). It may be of instrumental origin in the light of S/N ratios since the frequency range in concern is partly overlapped with the so-called 'MT dead band'. However, the possibility that real anisotropy in the conductivity structure beneath the PNG region caused the TM phase anomaly can not be excluded completely because anisotropy was not incorpolated in our 2D model studies.

In the course of our site-independent GB decomposition, sites PNG102, 121 and 122 were omitted because the χ^2 misfits of the three sites were statistically insignificant. However, we do not have any alternative at present other than abandoning the data from the statistically insignificant sites so far as we stick to the existing decomposition schemes. It might be time for us to introduce more sophisticated 'physics' into our decomposition models to avoid extraordinary large or 'biased' χ^2 misfits. In this sense, it may be safer to build in robustness in our decomposition schemes themselves though elimination of simple isolated outliers and/or local non-stationarity can now be easily accomplished in the course of response function estimation using robust codes (CHAVE et al., 1987).

5. Conclusions

The regional 2D strike angle of the PNG dataset was determined as 30° by site- and frequency-independent GB decomposition using data from seven selected sites though it was essential for our site-independent GB decomposition to make statistical examination of the χ^2 misfits derived by the frequency-independent GB decomposition at each site.

Two points can be commented here for future work in terms of improvement in finding the true regional 2D strike angle of a given MT dataset:

(1) The simple global χ^2 misfit minimization presented in this paper can be extended to a more complex regulated minimization such as ABIC minimization that includes both the misfit term and a priori information. This will yield a superior estimate to that of the simple misfit minimization if we stick to the existing decomposition schemes.

(2) It will be very useful to introduce new physics into the exisiting decomposition models if we're tired out using them. Built-in-robustness may be among clues to the 'new' decomposition scheme since it may reduce the influence of bad data points that do exist exclusively in any geophysical datasets.

We're grateful to Drs. Charles Swift and Alan G. Jones for providing us the PNG dataset. The GB decomposition code was made available to us via 'mtnet.europe'.

REFERENCES

BAHR, K., Interpretation of the magnetotelluric impedance tensor: Regional induction and local telluric distortion, *J. Geophys.*, **62**, 119-127, 1988.

BAHR, K., Geological noise in magnetotelluric data: A classification of distortion types, *Phys. Earth Planet. Inter.*, **66**, 24-38, 1991.

CHAVE, A. D., D. J. THOMSON and M. E. ANDER, On the robust estimation of power spectra, coherences, and transfer functions, *J. Geophys. Res.*, **92**, 633-648, 1987.

GROOM, R. W. and R. C. BAILEY, Decomposition of magnetotelluric impedance tensors in the presence of local three-dimensional galvanic distortion, *J. Geophys. Res.*, **94**, 1913-1925, 1989.

GROOM, R. W. and R. C. BAILEY, Analytic investigations of the effects of near-surface three-dimensional galvanic scatterers on MT tensor decompositions, *Geophysics*, **56**, 496-518, 1991.

GROOM, R. W. and K. BAHR, Corrections for near surface effects: Decomposition of the magnetotelluric impedance tensor and scaling corrections for regionalresistivities: A tutorial, *Surv. Geophys.*, **13**, 341-379, 1992.

GROOM, R. W., R. D. KURTZ, A. G. JONES and D. E. BOERNER, A quantitative methodology to extract regional magnetotelluric impedances and determine the dimension of the conductivity structure, *Geophys. J. Int.*, **115**, 1095-1118, 1993.

JONES, A. G., R. W. GROOM and R. D. KURTZ, Decomposotion and modelling of the BC87 dataset, *J. Geomag. Geoelectr.*, **45**, 1127-1150, 1993.

JONES, A. G. and R. W. GROOM, Strike angle determination from the magnetotelluric tensor in the presence of noise and local distortion: Rotate at your peril !, *Geophys. J. Int.*, **113**, 524-534, 1993.

TOH, H. and M. UYESHIMA, Two-dimensional model study of the PNG dataset using site-independent Groom-Bailey decomposition, *submitted to J. Geomag. Geoelectr.*, 1995.

UCHIDA, T., Smooth 2-D inversion for magnetotelluric data bsed on statistical criterion ABIC, *J. Geomag. Geoelectr.*, **45**, 841-858, 1993.

UTADA, H., A direct inversion method for two-dimensional modeling in the geomagnetic induction problem, Ph. D. Thesis, Univ. Tokyo, 409pp., 1987.

Figure Captions

Fig. 1. Site map of the PNG dataset. The profile is running in the SSW-NNE direction from site PNG108 to PNG121, whose length is as short as 5.6 km. Altitudes of each site are also shown.

Fig. 2. Traditional skewness (upperleft), Swift's angle (lowerleft), polar diagrams (upperright) and anisotropy ellipses (lowerright) at site PNG101, respectively. The polar diagrams and anisotropy ellipses are in arbitrary units and shown only for selected 4 frequencies.

Fig. 3. Same as Fig. 2 but for site PNG104. Note that Swift's angles at this site are unstable and frequency-dependent contrary to those of PNG101.

Fig. 4. Decomposed apparent resistivities and phase at site PNG102, that are rotated into the direction 30° clockwise from the north. Diamonds are those of TE mode and squares are TM mode while stars denote the arithmetic means of the two modes (the Berdichevsky averages). TM phases become abruptly very high between 10^{-1} and 10 Hz and even hit the 90° bound around 1 Hz.

Fig. 5. Results of frequency-dependent GB decomposition at site PNG122. (a) χ^2 misfits. (b) Twist, shear and 2D regional strike angles. (c) Observed Zxx and Zxy impedances (symbols with error bars; tiny crosses denote data whose lower error bounds give negative amplitudes.) and those predicted by the GB decomposition (solid lines). Note that the solid lines follow the outliers in Zxx amplitude and Zxy phase around 100 Hz.

Fig. 6. The 2D regional strike angle estimates of all 10 sites derived by frequency-independent GB decompositon at each site.

Fig. 7. χ^2 misfits derived by the frequency-independent GB decomposition at each site. The horizontal line corresponds to the line of 3σ allowance.

Fig. 8. Plot of 2D regional strike angles measured clockwise positive from the north vs. global χ^2 misfits derived by site-independent GB decomposition. This figure is the fundamental results of this study.

Fig. 9. Same plot as Fig. 5c at site PNG102 but for the fixed 2D strike angle of 30°. This figure gives the worst visual fit to the observed impedances after site-independent GB decomposition though the predicted values still stick to the observed values.

Site Locations of the PNG Dataset

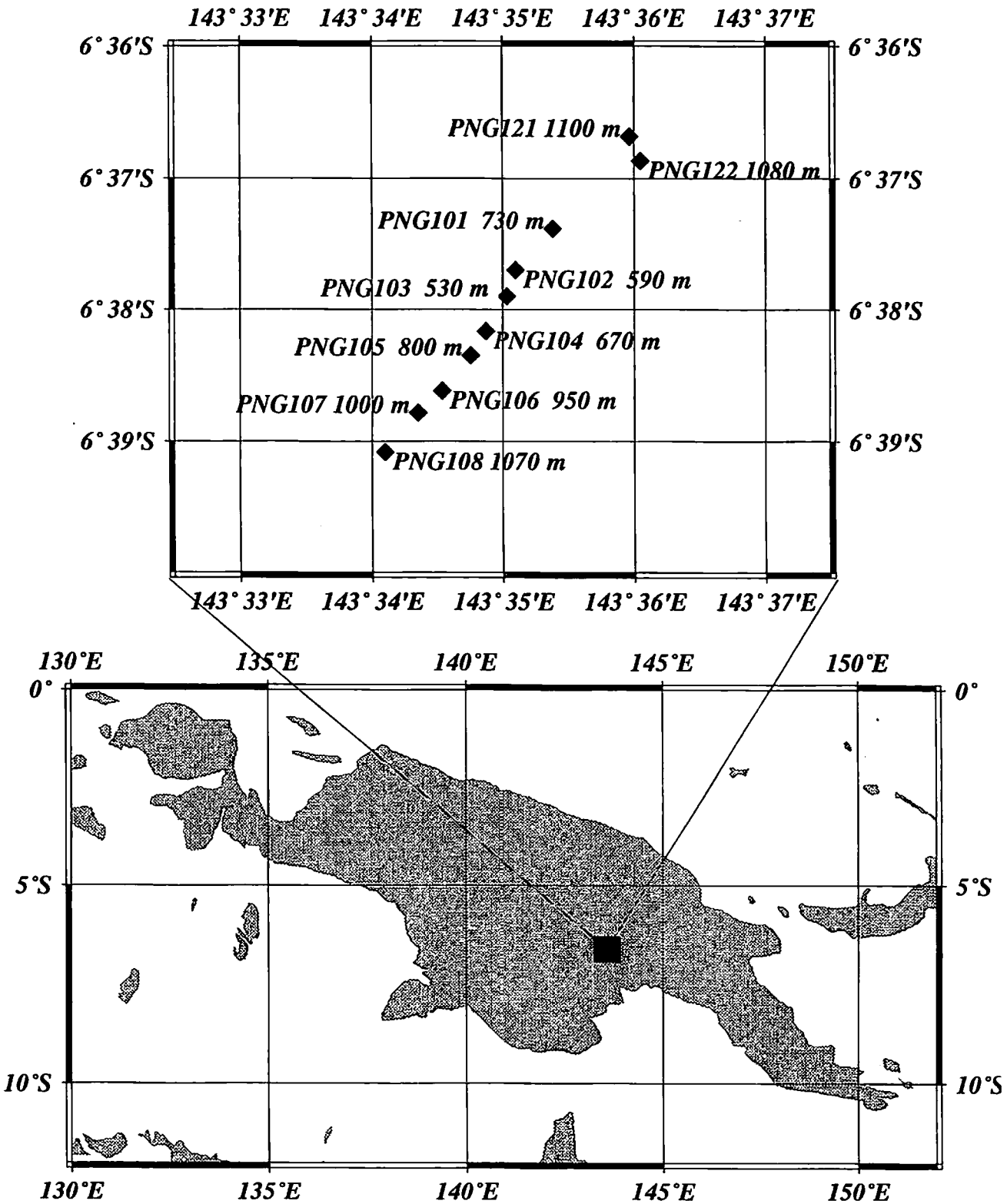

Skewness & Principal Direction

/hiroaki/toh/png/png101.impz

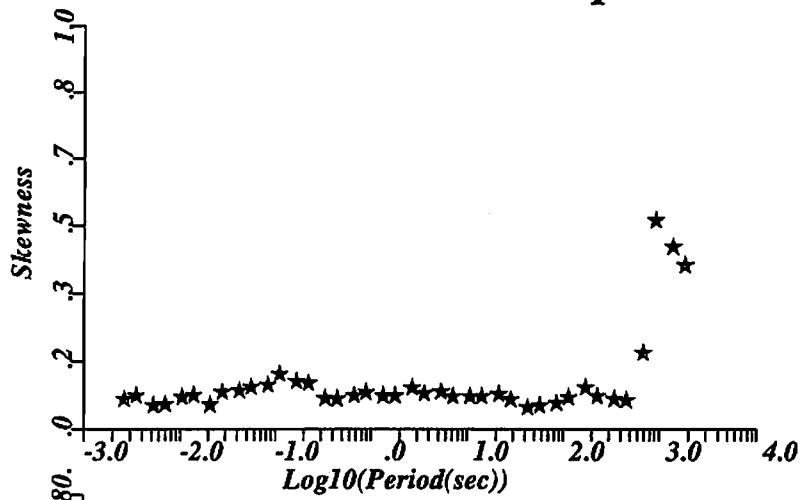

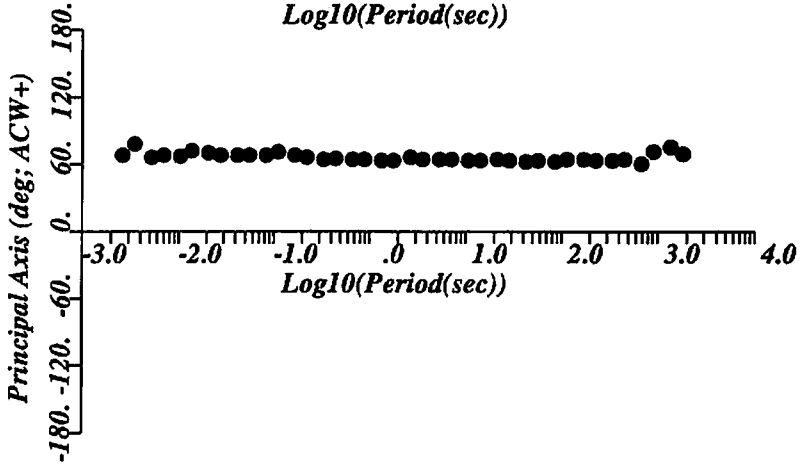

Polar Diagrams: Re(Zxx,Zxy)

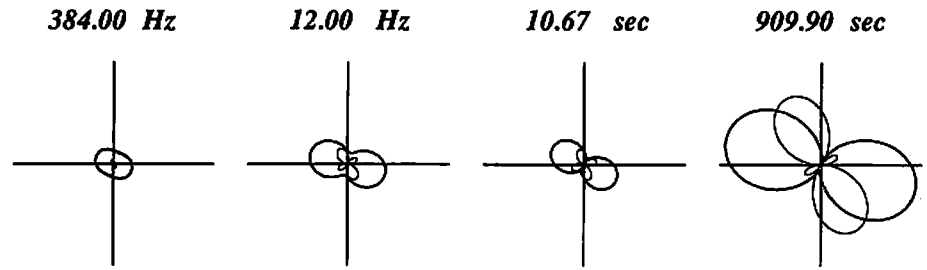

Anisotropy Ellipses

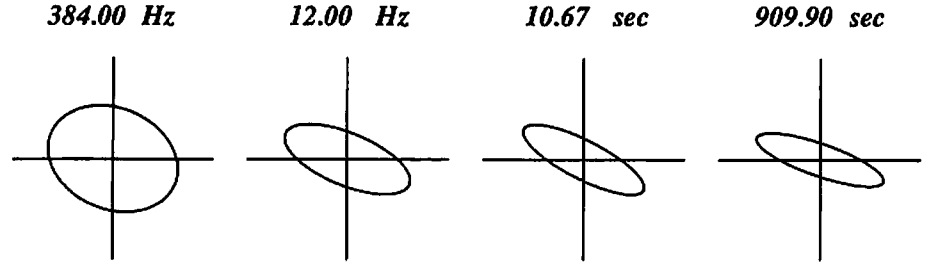

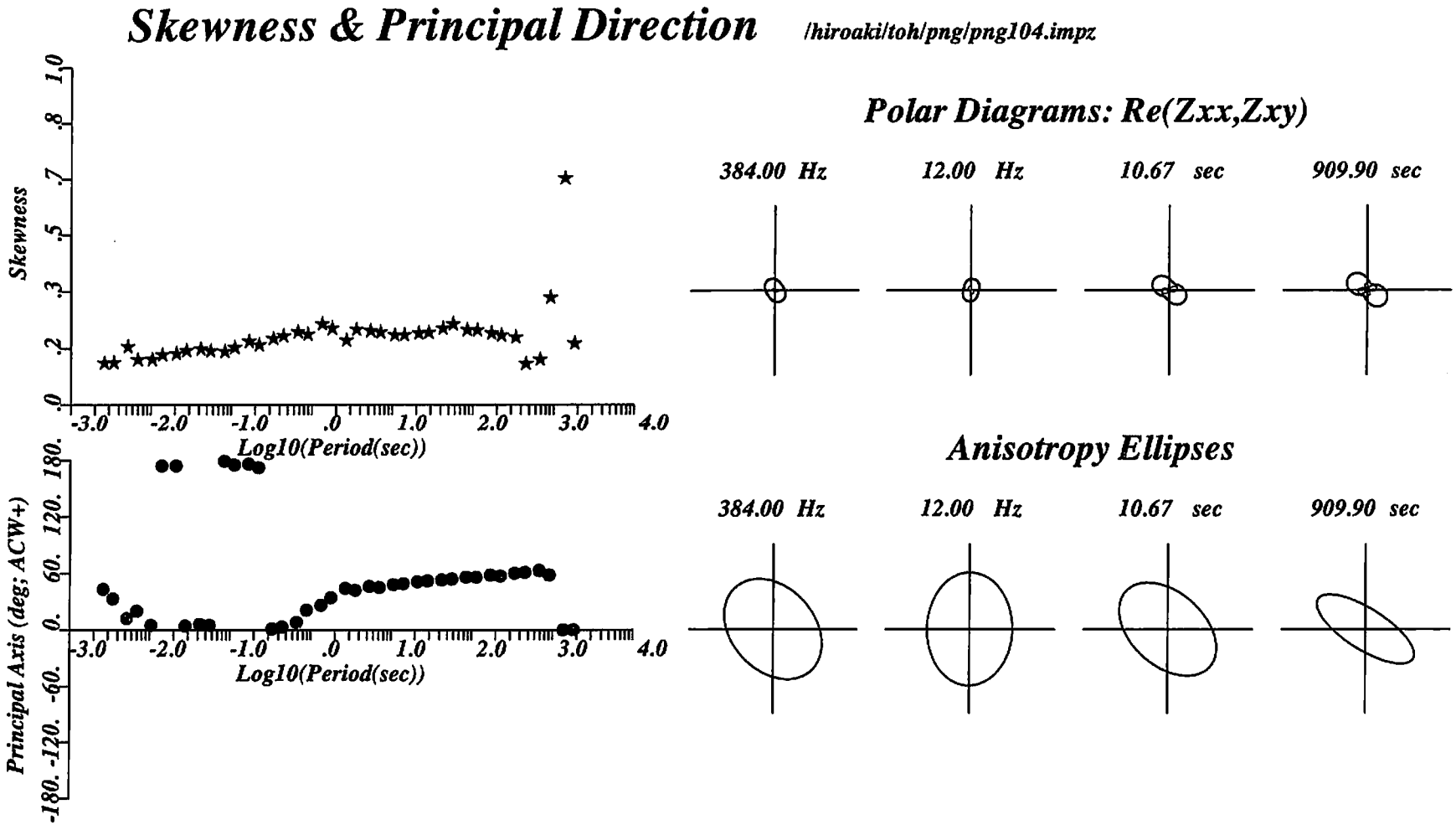
Skewness & Principal Direction
/hiroaki/toh/png/png104.impz
Skewness
1.0
.8
.7
.5
.3
.2
0
-3.0
-2.0
-1.0
.0
1.0
2.0
3.0
4.0
Log10(Period(sec))
Principal Axis (deg; ACW+)
180.
120.
60.
0.
-60.
-120.
-180.
Log10(Period(sec))
Polar Diagrams: Re(Zxx,Zxy)
384.00 Hz
12.00 Hz
10.67 sec
909.90 sec
Anisotropy Ellipses
384.00 Hz
12.00 Hz
10.67 sec
909.90 sec

Decomposed Apparent Resistivity & Phase

/hiroaki/toh/png/png102.a /hiroaki/toh/png/png102.b /hiroaki/toh/png/png102.avg

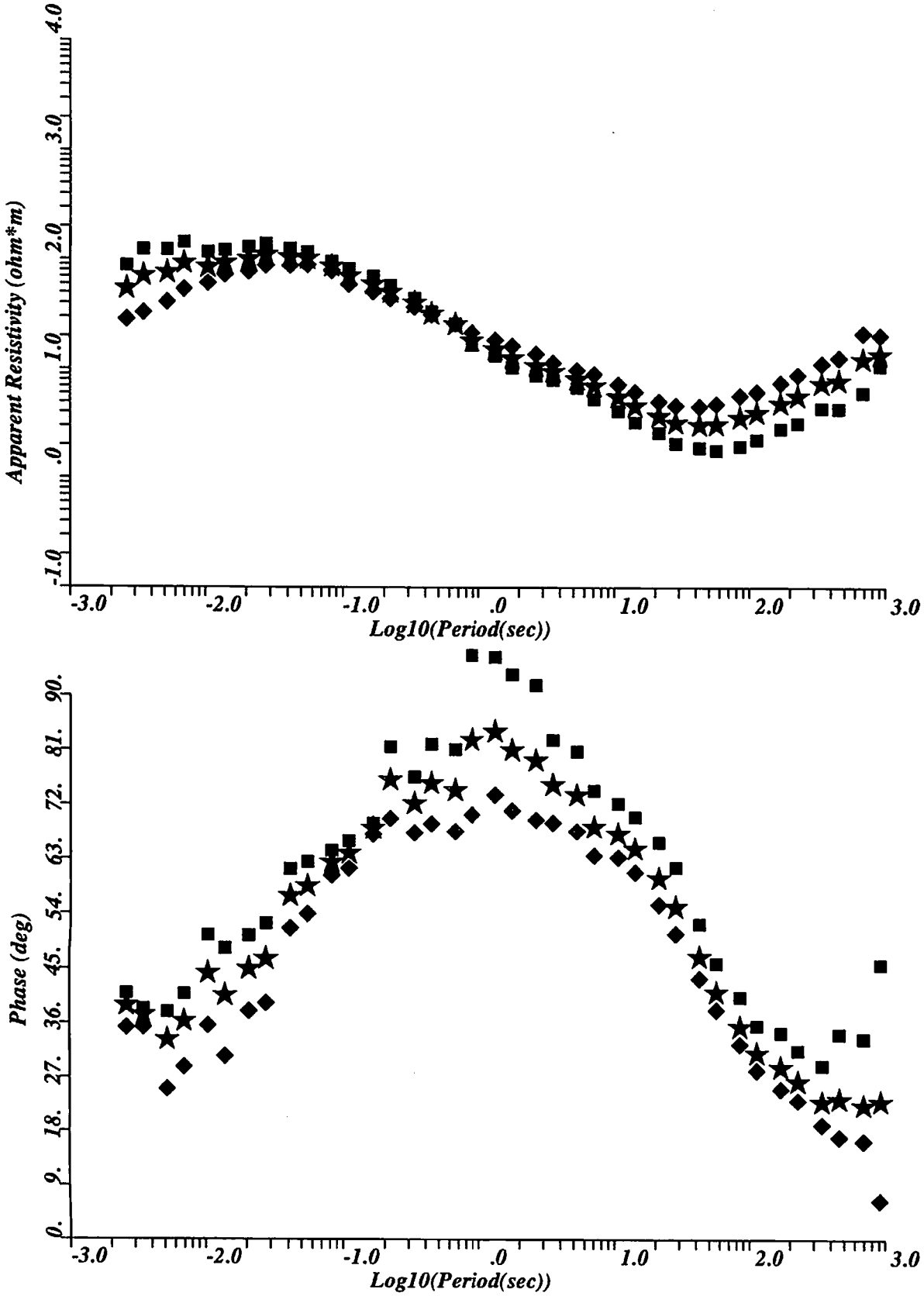

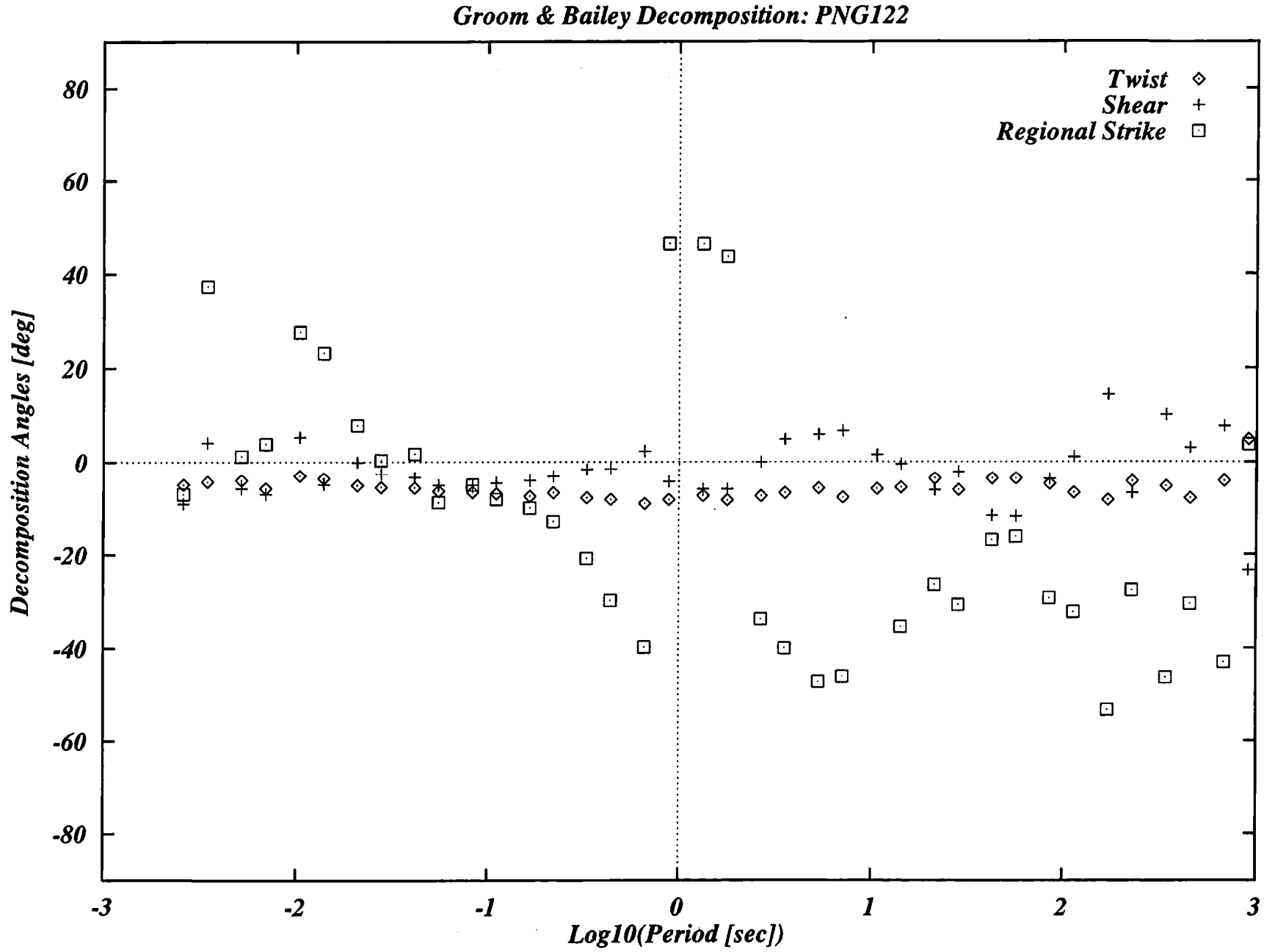
Groom & Bailey Decomposition: PNG122
Twist
Shear
Regional Strike
Decomposition Angles [deg]
80
60
40
20
0
-20
-40
-60
-80
-3
-2
-1
0
1
2
3
Log10(Period [sec])

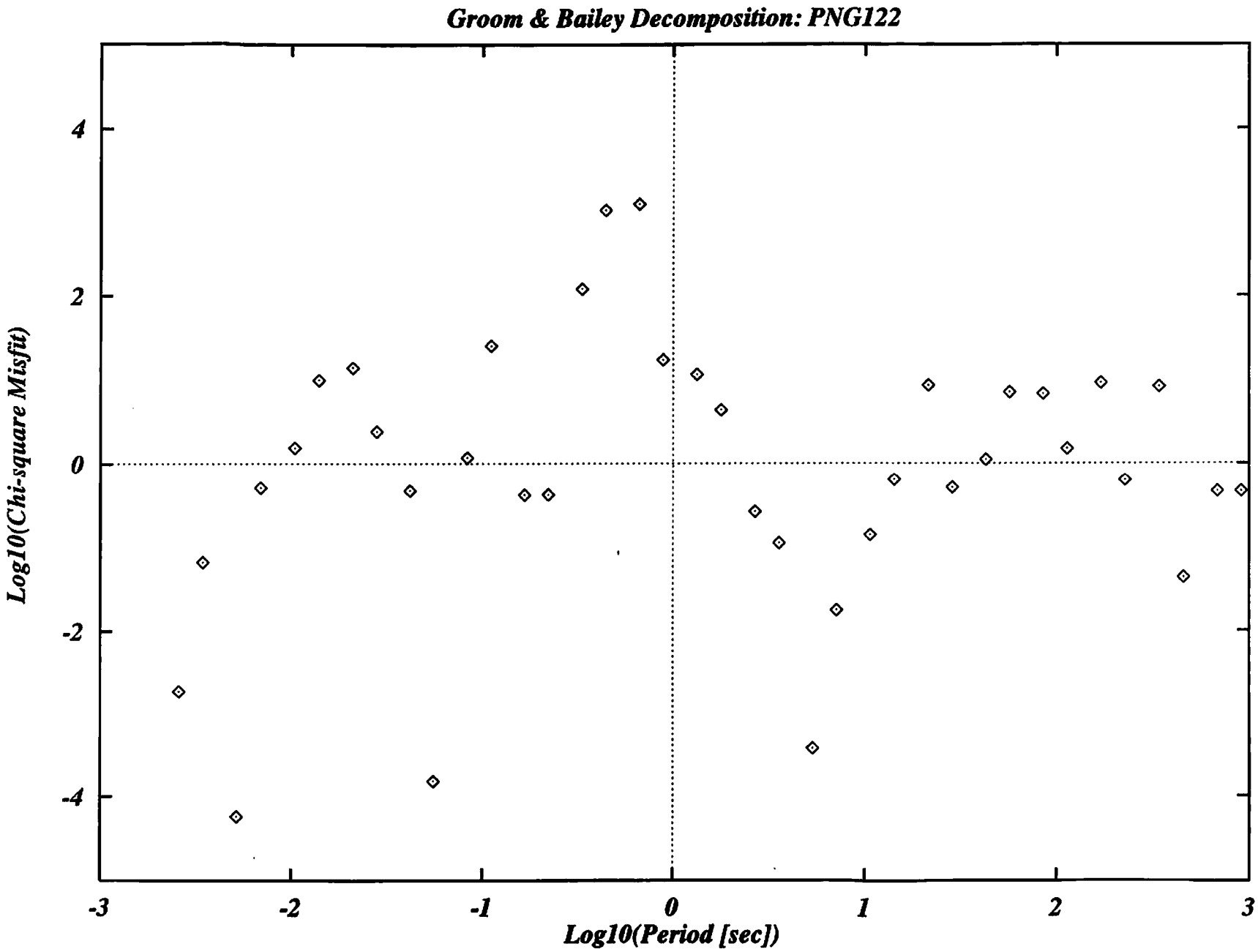
Groom & Bailey Decomposition: PNG122
Log10(Chi-square Misfit)
Log10(Period [sec])
4
2
0
-2
-4
-3
-2
-1
0
1
2
3

Predicted & Observed Impedances
/hiroaki/toh/png/png122.zxxzxy
/hiroaki/toh/png/png122.1r1.prf.fd
/hiroaki/toh/png/png122.1r2.prf.fd
Amplitude of Zxx (mV/km/nT)
Phase of Zxx (deg)
Amplitude of Zxy (mV/km/nT)
Phase of Zxy (deg)
Log10(Period(sec))

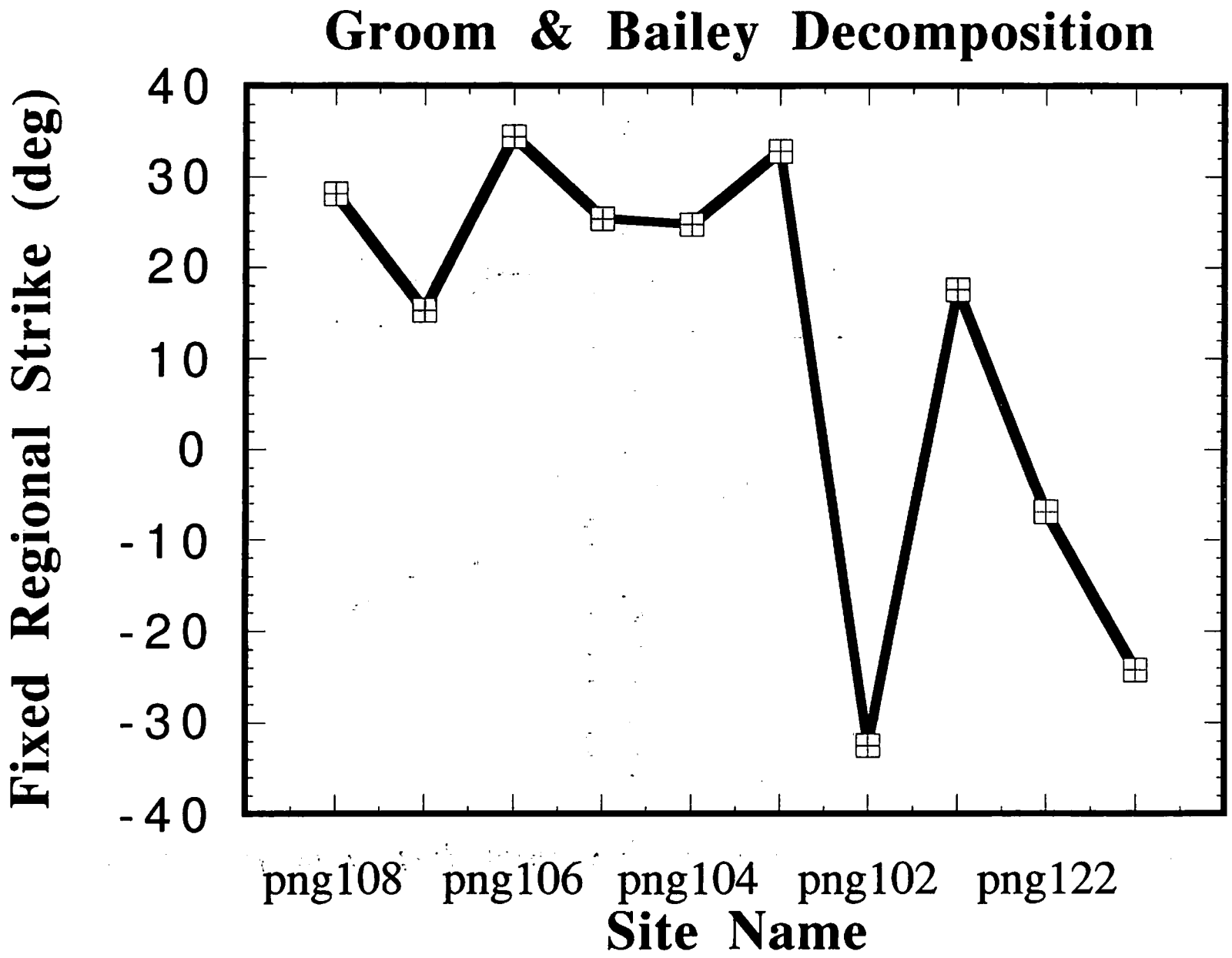
Groom & Bailey Decomposition
Fixed Regional Strike (deg)
40
30
20
10
0
-10
-20
-30
-40
png108
png106
png104
png102
png122
Site Name

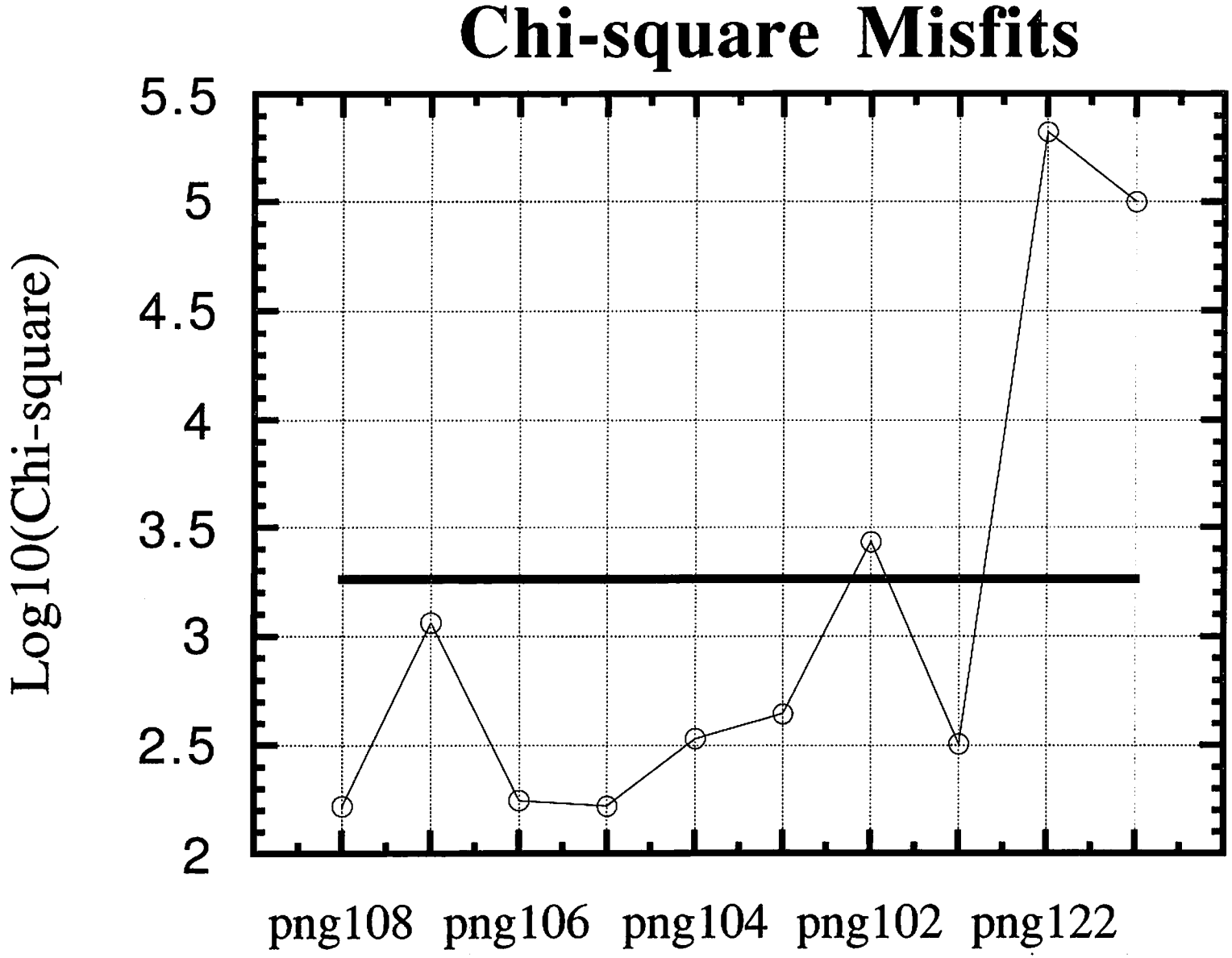
Chi-square Misfits
Log10(Chi-square)
5.5
5
4.5
4
3.5
3
2.5
2
png108
png106
png104
png102
png122

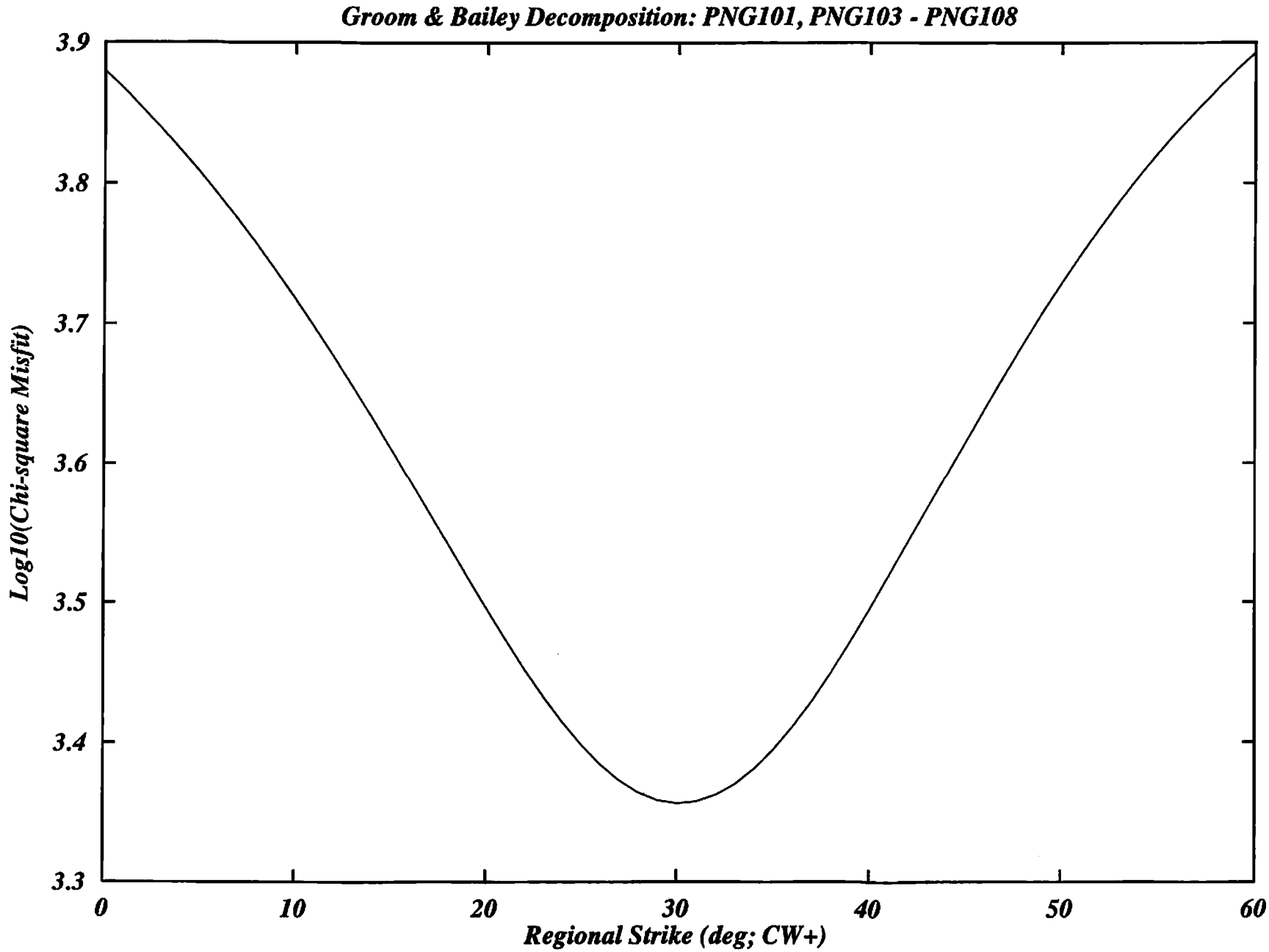
Groom & Bailey Decomposition: PNG101, PNG103 - PNG108
Log10(Chi-square Misfit)
3.9
3.8
3.7
3.6
3.5
3.4
3.3
0
10
20
30
40
50
60
Regional Strike (deg; CW+)

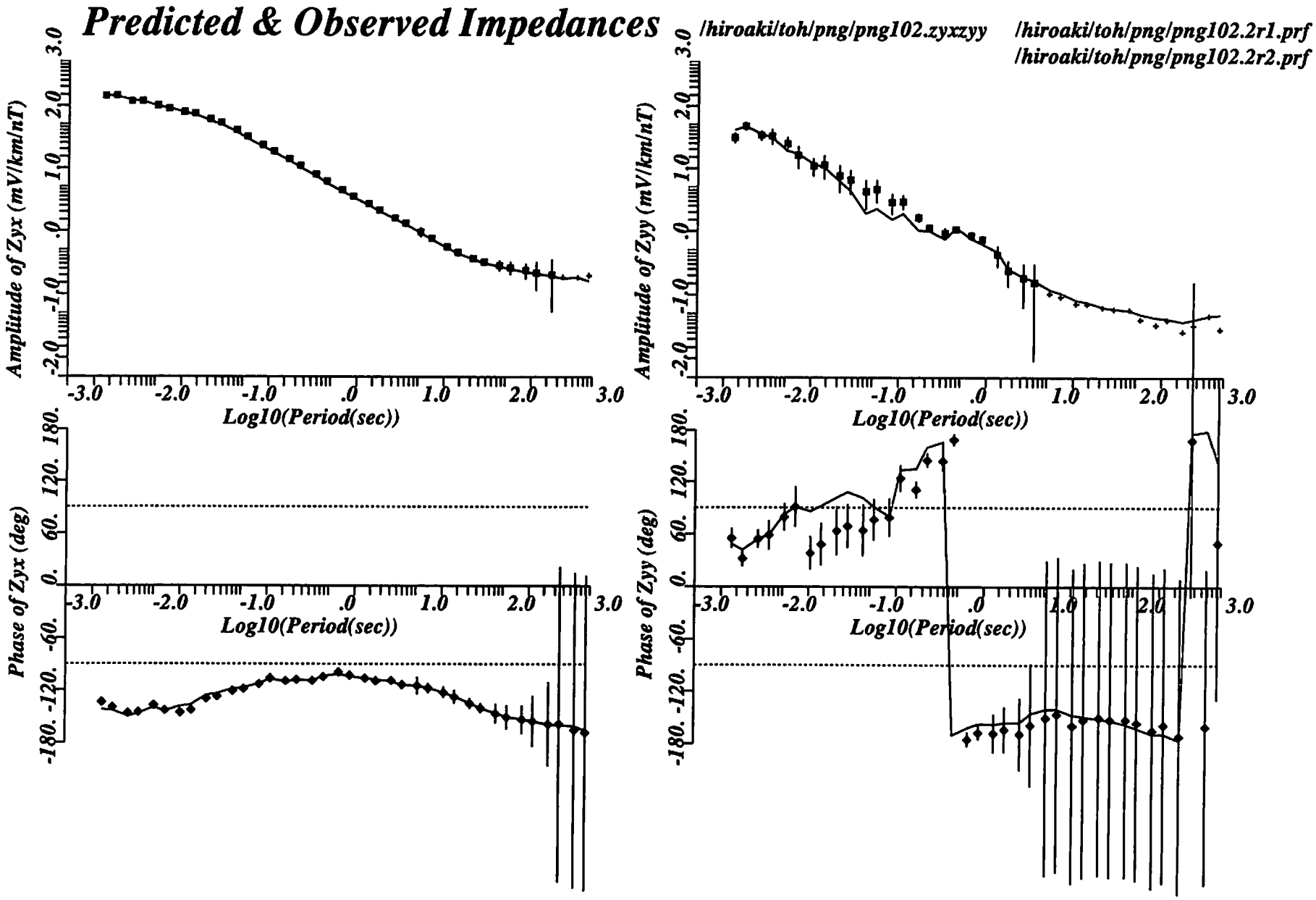
Predicted & Observed Impedances
/hiroaki/toh/png/png102.zyxzyy
/hiroaki/toh/png/png102.2r1.prf
/hiroaki/toh/png/png102.2r2.prf
Amplitude of Zyx (mV/km/nT)
Amplitude of Zyy (mV/km/nT)
Phase of Zyx (deg)
Phase of Zyy (deg)
Log10(Period(sec))
3.0
2.0
1.0
.0
-1.0
-2.0
180.
120.
60.
0.
-60.
-120.
-180.